Supporting Information for

Bringing earth-abundant plasmonic catalysis to the lights: Gram-scale mechanochemical synthesis and tunning of activity by dual excitation of antenna and reactor sites

Jhon Quiroz,[a+] Paulo F M de Oliveira,[b,c+] Shwetha Shetty,[a] Freddy E. Oropeza,[d] Víctor A. de la Peña O'Shea,[d] Lucas C. V. Rodrigues,[b] Maria P de S Rodrigues,[b] Roberto Manuel Torresi,[b] Franziska Emmerling,[c] and Pedro H. C. Camargo[a*]

[a]*Department of Chemistry, University of Helsinki, A.I. Virtasen aukio 1,* 00560, *Helsinki, Finland.*

[b]*Departamento de Química Fundamental, Instituto de Química, Universidade de São Paulo. Av. Lineu Prestes 748, 05508000, São Paulo, Brazil.*

[c]*BAM Federal Institute for Materials Research and Testing, Richard-Willstätter-Strasse 11, 12489 Berlin, Germany*

[d]*Photoactivated Processes Unit, IMDEA Energy Institute, Parque Tecnologico de Mostoles, 28935 Mostoles, Madrid, Spain*

*Corresponding author. Email: pedro.camargo@helsinki.fi

Number of pages: 11

Number of figures: 9

Number of tables: 1

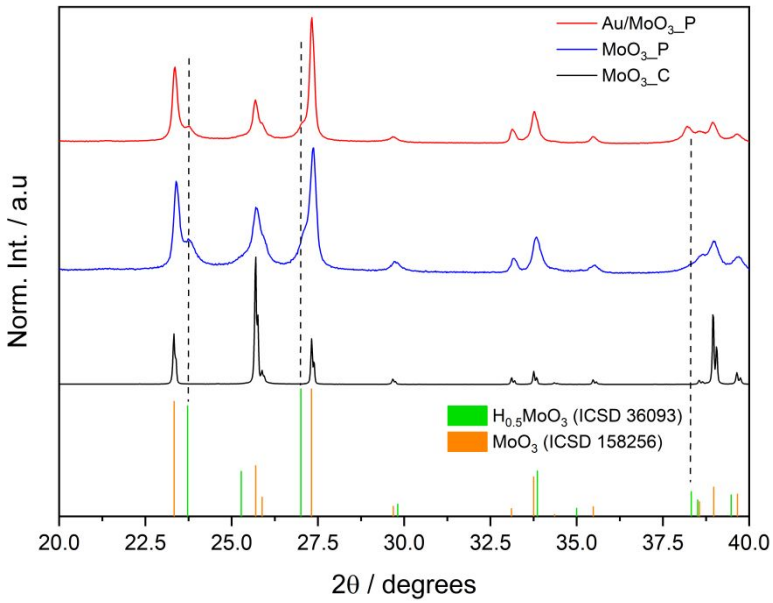

Figure S1. Normalized XRD diffractograms for commercial MoO_3 (MoO_3_C, black trace), plasmonic MoO_3 obtained after ball-milling in the presence of $NaBH_4$ (MoO_3_P, blue trace), and Au NPs supported onto plasmonic MoO_3 produced by ball-milling MoO_3 and AuCl in the presence of $NaBH_4$ (Au/MoO_3_P, red trace). The H0.5MoO3 phase can be clearly identified in the XRD patterns for MoO_3_P and Au/MoO_3_P.

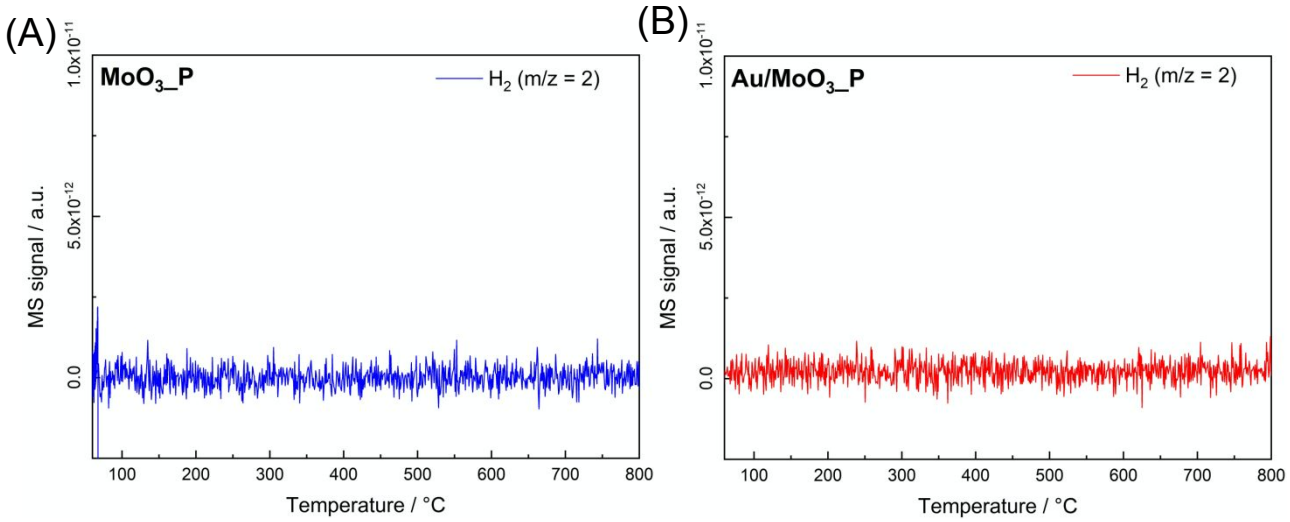

Figure S2. H_2 Temperature programmed desorption (TPD) for plasmonic MoO_3 sample obtained after ball-milling MoO_3 with $NaBH_4$ in the absence of AuCl, (MoO_3_P), and the Au/MoO_3_P samples (obtained after ball-milling MoO_3 with $NaBH_4$ and AuCl). In both cases, no peaks assigned to H_2 were detected.

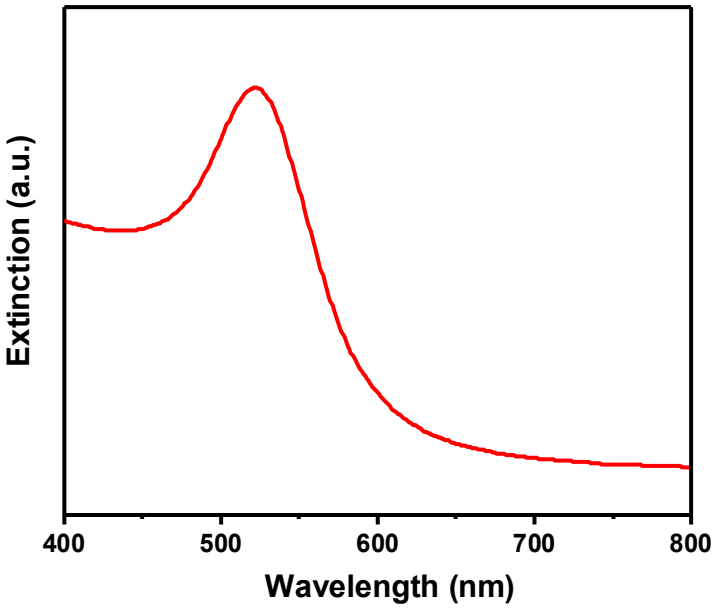

Figure S3. UV-VIS extinction spectrum recorded from an aqueous suspension containing Au NPs 15 nm in diameter.

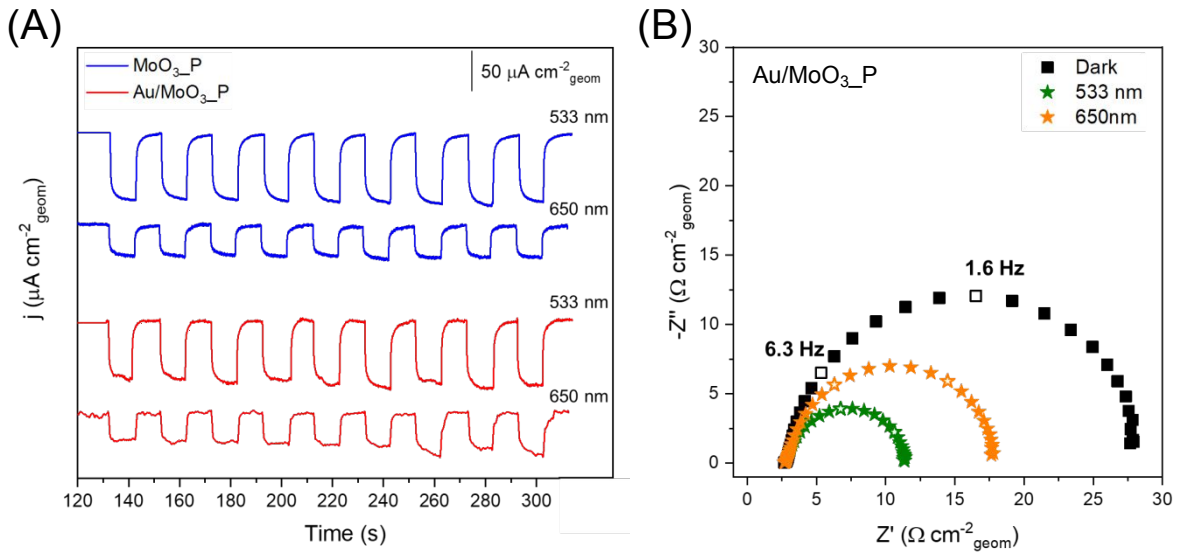

Figure S4. (A) On-off j-t transients under chopped illumination at 533 and 650 nm irradiation for MoO_3_P (blue trace) and Au/MoO_3_P (red trace) recorded at -0.45 V_{RHE} in N_2-saturated KOH 1 $molL^{-1}$ electrolyte and hydrodynamic conditions (1600 rpm). Both samples showed a fast and reproducible response to the on-off cycles towards the hydrogen evolution reaction (HER), with the highest photocurrents registered under 533 nm laser irradiation. (B) Nyquist plot for Au/MoO_3_P registered at -0.45V_{RHE} in the dark and under 650 and 533 nm illumination. The frequency varied from 10 mHz to 100 kHz. All measurements were performed in N_2-saturated KOH 1 $molL^{-1}$ and normalized by geometric area. The Au/MoO_3_P showed a remarkable decrease on the R_{ct} under light irradiation, starting in 27 W $_{cm}{}^2$ in dark condition and reaching 17 and 11 W $_{cm}{}^2$ for 650 and 533 nm, respectively. This decrease indicates that the most efficient interfacial electron transfer was reached under 533 nm illumination, which better matches the LSPR band for Au in Au/MoO_3_P.

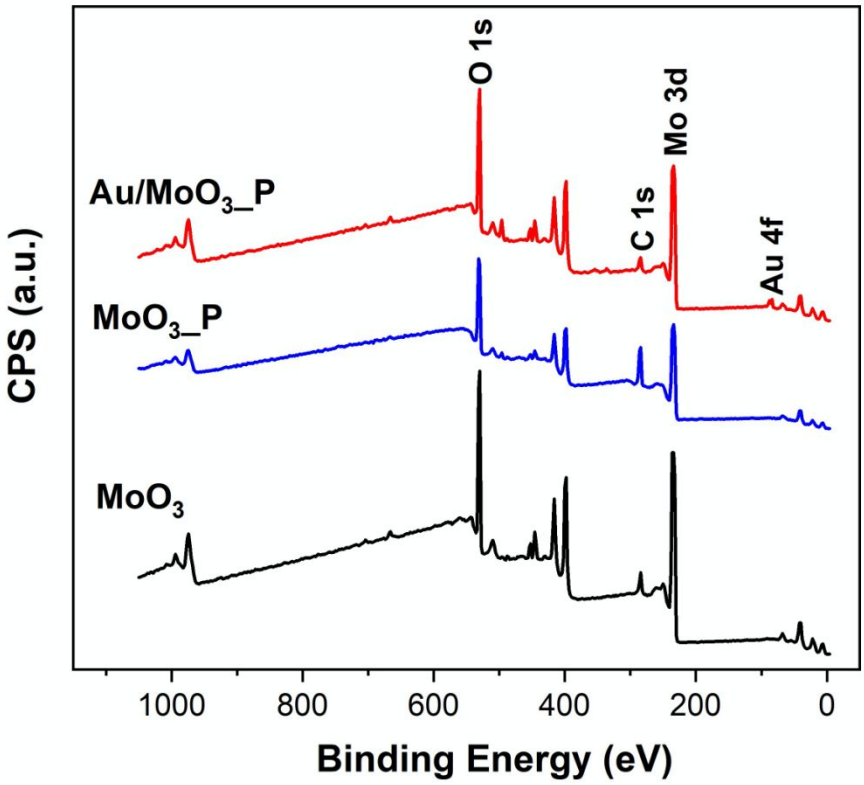

Figure S5. XPS survey spectra for commercial MoO_3 (MoO_3_C, black trace), plasmonic MoO_3 obtained after ball-milling in the presence of $NaBH_4$ (MoO_3_P, blue trace), and Au NPs supported onto plasmonic MoO_3 produced by ball-milling MoO_3 and AuCl in the presence of $NaBH_4$ (Au/MoO_3_P, red trace).

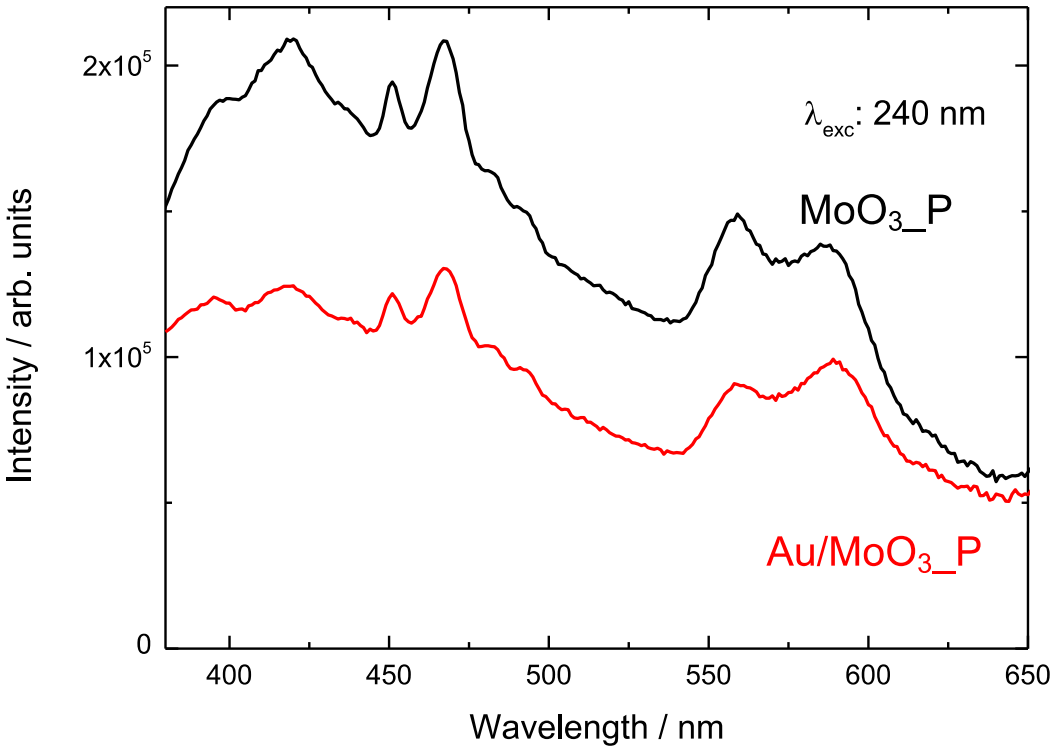

Figure S6. Photoluminescence (PL) spectra recorded at room temperature for plasmonic MoO_3 sample obtained after ball-milling MoO_3 with $NaBH_4$ in the absence of AuCl, (MoO_3_P), and the Au/MoO_3_P samples (obtained after ball-milling MoO_3 with $NaBH_4$ and AuCl).

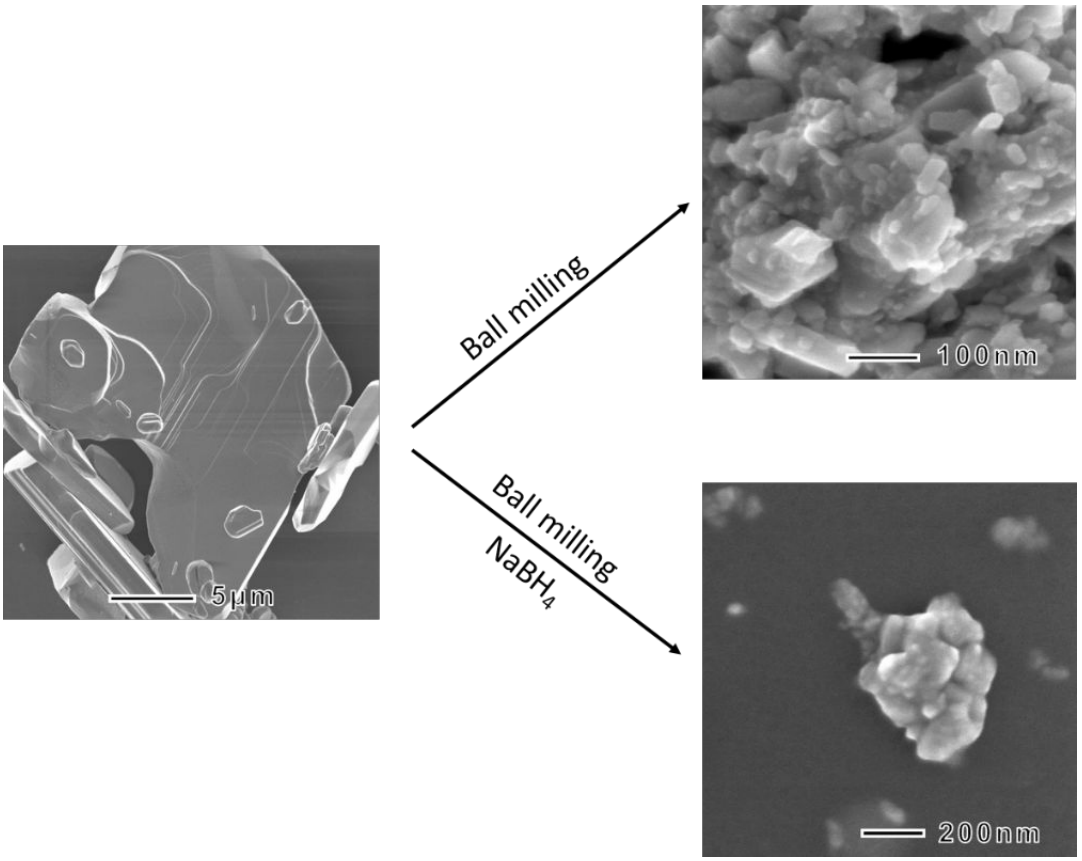

Figure S7. Scanning electron microscopy (SEM) image of commercial MoO_3 (left), commercial MoO_3 after ball milling in the absence of $NaBH_4$ (right, top panel), and commercial MoO_3 before and after ball billing in the presence of $NaBH_4$ (right, bottom panel).

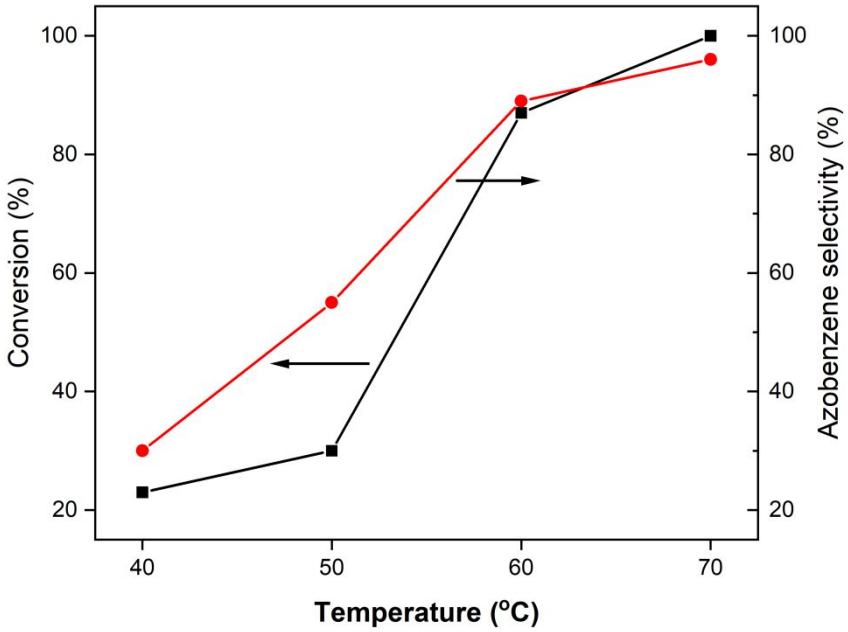

Figure S8. Nitrobenzene conversion (black trace) and azobenzene selectivity (red trace) as a function of the reaction temperature catalyzed by Au/MoO_3_P. The reactions were carried out by dual illumination with 530 nm and 740 nm lamps.

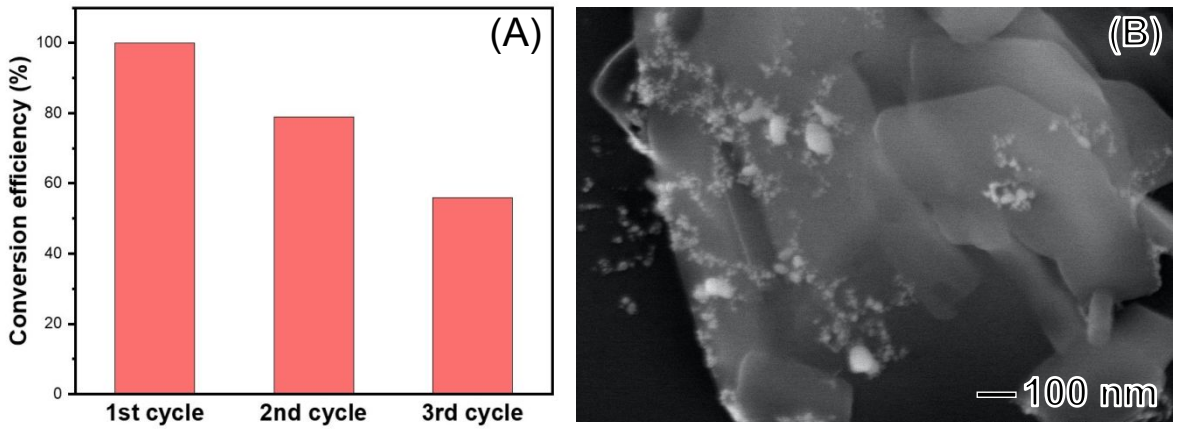

Figure S9. (A) Recycling/stability studies employing Au/MoO3_P as plasmonic catalysts under the same conditions as described Table 2, entry 4. (B) SEM images of Au/MoO3_P after the recycling/stability studies described in (A), suggesting significant morphological changes.

Table S1. Hydrogenation if nitrobenzene Oxidation of Benzene under plasmonic excitation for Au/MoO_3_P and other catalysts reported in literature. The TOF values were calculated based on the gold loading.

Catalyst	Au loading (wt%)	Temperature (°C)	Conversion %	TOF (h^{-1})	Ref.
Au/MoO_3_P	5.0	70	100	33	this paper
Au/ZrO_2	1.5	40	59	47	1
Au/Al_2O_3	2.0	23	100	18	2
Au/CeO_2	3.0	30	43.5	43	3
Au/TiO_2	4.3	25	95	4	4
$AgCu/ZrO_2$	3.0	60	96	2	5

(1) Zhu, H.; Ke, X.; Yang, X.; Sarina, S.; Liu, H. Reduction of Nitroaromatic Compounds on Supported Gold Nanoparticles by Visible and Ultraviolet Light. *Angew. Chem. Int. Ed.* **2010**, *49* (50), 9657–9661. https://doi.org/10.1002/anie.201003908.

(2) Chaiseeda, K.; Nishimura, S.; Ebitani, K. Gold Nanoparticles Supported on Alumina as a Catalyst for Surface Plasmon-Enhanced Selective Reductions of Nitrobenzene. *ACS Omega* **2017**, *2* (10), 7066–7070. https://doi.org/10.1021/acsomega.7b01248.

(3) Ke, X.; Zhang, X.; Zhao, J.; Sarina, S.; Barry, J.; Zhu, H. Selective Reductions Using Visible Light Photocatalysts of Supported Gold Nanoparticles. *Green Chem.* **2013**, *15* (1), 236–244. https://doi.org/10.1039/c2gc36542a.

(4) Naya, S. I.; Niwa, T.; Kume, T.; Tada, H. Visible-Light-Induced Electron Transport from Small to Large Nanoparticles in Bimodal Gold Nanoparticle-Loaded Titanium(IV) Oxide. *Angew. Chem. Int. Ed.* **2014**, *53* (28), 7305–7309. https://doi.org/10.1002/anie.201402939.

(5) Liu, Z.; Huang, Y.; Xiao, Q.; Zhu, H. Selective Reduction of Nitroaromatics to Azoxy Compounds on Supported Ag-Cu Alloy Nanoparticles through Visible Light Irradiation. *Green Chem.* **201AD**, *18* (3), 817–825. https://doi.org/10.1039/x0xx00000x.